https://doi.org/10.5194/wes-2025-258
Preprint. Discussion started: 25 November 2025

Wind turbine performance and control in complex terrain

Clemens Paul Zengler[1], Mac Gaunaa[1], and Niels Troldborg[1]

[1]Department of Wind and Energy Systems, Technical University of Denmark. Frederiksborgvej 399, 4000 Roskilde, Denmark

Correspondence: Clemens Paul Zengler (clezen@dtu.dk)

Abstract. Wind energy projects in complex terrain are often associated with high uncertainties regarding the expected power performance. These uncertainties are mostly attributed to difficulties in obtaining reliable wind speed estimates. However, an additional factor is that the physical limits of energy extraction vary in these cases, and that the employed wind turbine might operate differently than expected in these conditions. Reynolds-averaged Navier-Stokes (RANS) simulations of a wind turbine modeled as an actuator disk (AD) subject to a neutral atmospheric inflow are performed. The influence of the turbine position relative to a quasi-two-dimensional Gaussian hill on the maximum power performance and on the response of a torque controller in region ~~two~~ of the power curve is investigated. When the turbine is located at the foot of the hill, the maximum power coefficient increases by 3.5%. At the top of the hill, the maximum power decreases by 20.0%. A consequence of this is that, when placing wind turbines on elevated locations, the power does not scale with the cube of the increase of wind speed. It is furthermore found~~,~~ that the torque controller operates in a way, that local flow angles remain constant, irrespectively of the location of the turbine. Also, the power coefficient based on the disturbed wind speed in the rotor plane remains constant, which does not necessarily coincide with the maximum power coefficient based on the undisturbed wind speed. As a consequence, a torque controller does not track maximum performance in complex terrain. Overall, this study sheds light on the interpretation of performance results of wind turbines in complex terrain and helps to shape efforts to decrease prediction uncertainties for future onshore wind projects.

1 Introduction

Wind turbine control can be roughly divided into three regions depending on the wind speed. In region one, no power is extracted, in region two, the primary objective is to maximize energy extraction from the flow field, and in region three, the power generation is kept constant. An example of a power curve with these three regions and the respective rotor speed and collective blade pitch is presented in Fig. 1. Also, regions 1.5 and 2.5 are shown, which are commonly used to set a minimum rotor speed and to reduce loads and noise (Abbas et al., 2022). In this work, we focus solely on analyzing region two from an aerodynamic perspective, where it is traditionally attempted to maintain a constant power and thrust coefficient to primarily extract as much energy as possible from the flow. Nonetheless, for the sake of completeness, the other regions are included in the simulations as well.

~~But~~ what is actually the available energy in the flow? Recent research has shown that using only local hub position quantities, like the free wind speed, is insufficient to quantify this energy content, but also the streamwise development of the free wind

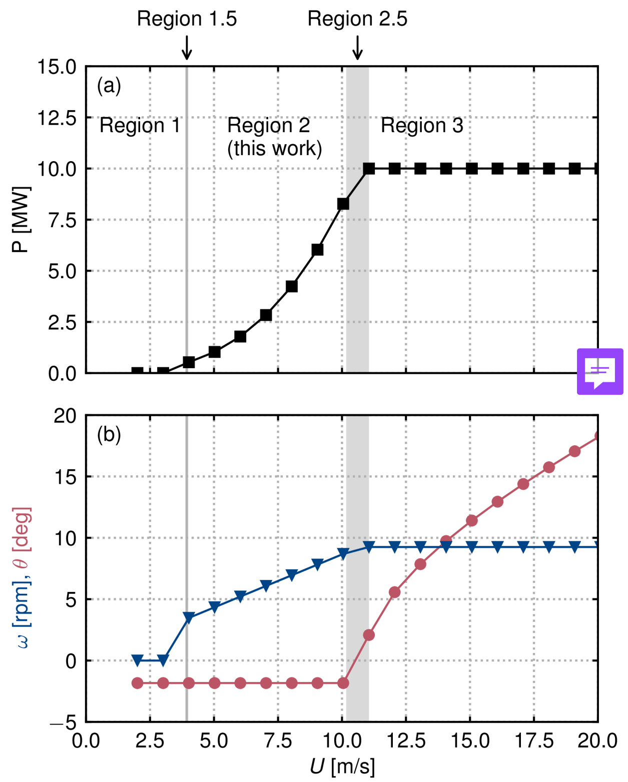

Figure 1. An example of a power curve of a wind turbine with the different control regions labeled: (a) Power and (b) rotor speed ω and blade pitch θ.

speed needs to be taken into account (Troldborg et al., 2022; Zengler et al., 2024; Revaz and Porté-Agel, 2024). In other words, the location of a wind turbine and the development of the flow around this location affect the power performance. A streamwise acceleration of the flow leads to an increase of power, while a deceleration leads to a decrease (Dar et al., 2023). On the one side, power performance models that consider this effect are solely based on conservation equations (Cai et al., 2021; Zengler et al., 2025a; Dar et al., 2025) without considering the controller. And on the other side, studies on wind turbine performance in complex terrain often rely on certain controllers (Revaz and Porté-Agel, 2024; Liu and Stevens, 2020) without actively investigating the influence of the control choice on performance results. This makes it difficult to draw ~~definite~~ conclusions from these studies, because the exact interaction between controller and non-uniform background flow is not clear.

A common way of controlling a wind turbine in region ~~two~~ of the power curve uses a torque controller, which sets the generator torque to enforce the appropriate equilibrium between generator and rotor torque (Bossanyi, 2000; Pao and Johnson, 2011). It relies on the rotational speed of the rotor as input, which, unlike wind speed, can be easily measured in both real life and simulation environments. To derive the torque control law, we start with the power which can be calculated for a given wind speed U_{Ref} as

$$P = \frac{1}{2}\rho R^2 \pi C_P(\lambda,\theta,X)\,U_{\mathrm{Ref}}^3, \tag{1}$$

with air density ρ, rotor radius R, and power coefficient C_P which depends on the tip-speed ratio $\lambda = \omega R/U_{\mathrm{Ref}}$, the blade pitch θ, and also on the location X, as the aforementioned research shows. In the following, these dependencies will not be explicitly mentioned. The rotor torque is related to the power as

$$\tau = \frac{P}{\omega} = \frac{1}{2}\rho R^2 \pi C_P \frac{U_{\mathrm{Ref}}^3}{\omega}, \tag{2}$$

In order to design a torque controller, it is desired to keep the local flow angles at the blade constant at the conditions, where maximum $C_{P,\mathrm{max}}$ is reached. This means that the tip-speed ratio must remain constant. By substituting $U_{\mathrm{Ref}} = \omega R/\lambda_{\mathrm{opt}}$, one obtains (Bossanyi, 2000; Bianchi et al., 2007)

$$\tau = \underbrace{\frac{1}{2}\rho R^5 \pi \frac{C_{P,\mathrm{max}}}{\lambda_{\mathrm{opt}}^3}}_{k}\,\omega^2 = k\omega^2, \tag{3}$$

where the torque constant k is introduced. This equation can now be used to set the generator torque τ_{Gen} as a function of the rotor speed to ensure optimal operation. As the name suggests, k is kept constant in this case, representing optimal operation in the environment the controller was calibrated for. The substitution of U_{Ref} in order to maintain constant local flow angles is essential to understand how a torque controller works from an aerodynamic perspective. Of course, the controller does not track the local flow angles. But maintaining $\tau \propto \omega^2$ is from an aerodynamic perspective only possible when aerodynamic ~~forces~~ also scale with the rotor speed squared, which is only the case, when local flow angles are kept constant This will become apparent in the course of this paper. For now, we will adhere to the traditional approach of evaluating wind turbine performance in terms of power coefficient and tip-speed ratio. In steady state, conservation of angular momentum between the rotor and the generator yields

$$\tau_{\mathrm{Gen}} = \tau_{\mathrm{Aero}} \Leftrightarrow k\omega^2 = \frac{1}{2}\rho R^5 \pi \frac{C_P}{\lambda^3}\omega^2 \Leftrightarrow \frac{C_{P,\mathrm{max}}}{\lambda_{\mathrm{opt}}^3} = \frac{C_P}{\lambda^3}. \tag{4}$$

This means that for our example of a turbine in flat terrain, the turbine will always track the curve defined by $\frac{C_{P,\mathrm{max}}}{\lambda_{\mathrm{opt}}^3} = \frac{C_P}{\lambda^3}$.

In computational fluid dynamics (CFD), an alternative to this type of control is to set the rotor speed (and also the blade pitch) directly as a function of the wind speed in the rotor plane during operation of the turbine based on a calibration procedure carried out in advance (van der Laan et al., 2014). It was previously shown that this approach is equivalent to a torque controller in region two because in this region, rotational speed and disk velocity are linked by a constant (Zengler et al., 2025b).

The derivation of the torque control law indicates that the power coefficient is an essential part of the control design. However, it also depends on the background flow, raising the question of what impact a controller tuned to flat terrain has on the performance of ~~the~~ turbine located in complex terrain. This study seeks to entangle controller and complex terrain effects and therefore contribute to a deeper understanding of simulation results and turbine operation in complex terrain. For this purpose,

https://doi.org/10.5194/wes-2025-258
Preprint. Discussion started: 25 November 2025

the steady-state control of a wind turbine in streamwise non-uniform flow fields is investigated through CFD simulations of an actuator disk (AD) located at different positions relative to a hill, and the results are discussed based on theoretical considerations. To the knowledge of the authors, this work for the first time investigates the influence of streamwise non-uniformity of the flow field on wind turbine control. The work is structured as follows: Sec. 2 presents the methodology which is largely based on previous works, Sec. 3 presents the results and Sec. 4. discusses the results and put them in a broader context.

2 Methodology

Simulations of a turbine in three different terrain setups are considered as shown in Fig. 2. In the first case (**A**), the turbine is operating in flat terrain, with no obstacles present. In the second case (**B**), the turbine is located at the foot of a hill, which accelerates the wake flow. The hill itself is quasi-two-dimensional parametrized by a Gaussian function. In the last case (**C**), the turbine is located on the ridge of the hill, which results in a deceleration of the wake. For the last case, additional simulations with varying hill height, width and surface roughness are performed. These are not analyzed in detail but serve as support for arguments made in the discussion presented in Sec. 4. The direction of the onset wind is perpendicular to the ridge of the hill, resulting in a quasi-two-dimensional flow field when the turbine is not operating. In general, the setup is similar to the one described by Zengler et al. (2024), employing Reynolds-averaged Navier-Stokes (RANS) simulations of a neutral atmospheric inflow.

2.1 Turbine model

The blade geometries of the DTU 10 MW ~~RWT~~ with a rotor diameter of 178.3 m and a hub height of 119 m are used for the simulations (Bak et al., 2013).

2.2 Controller

A traditional pitch-torque control algorithm as described by Jonkman et al. (2009) is used to control the rotational speed of the turbine. As mentioned before, the generator torque in region ~~two~~ is calculated as

$$\tau_{\mathrm{Gen}} = k\omega^2, \tag{5}$$

where the torque constant k is

$$k = \frac{1}{2}\rho\pi R^5 \frac{C_{P,\mathrm{max}}}{\lambda_{\mathrm{opt}}^3}. \tag{6}$$

The values of $C_{P,\mathrm{max}}$ and λ_{opt} are obtained from the simulated flat terrain C_P-λ-pitch surface ~~later~~ presented in Fig. 2 at the blade pitch θ_{opt} ~~which~~ maximizes the power coefficient. In every iteration i of the simulation, ω is updated until convergence based on the conservation of angular momentum of the rotor as

$$\omega_{i+1} = \omega_i + \frac{\Delta t}{J}\left(\tau_{\mathrm{Aero},i} - \tau_{\mathrm{Gen},i}\right), \tag{7}$$

https://doi.org/10.5194/wes-2025-258
Preprint. Discussion started: 25 November 2025

with the pseudo-time step Δt, the rotor moment of inertia J and the aerodynamic torque $\tau_{\mathrm{Aero},i}$, which is extracted from the flow simulation. A low-pass filter for the rotational speed is used in Eq. (7) as described by Jonkman et al. (2009). In ~~a~~ steady state, aerodynamic and generator torque need to be in balance, which ensures that below rated wind speed in flat terrain, the turbine tracks maximum power performance. Because steady-state simulations are performed, the dynamic response of the controller is not of interest here and $\Delta t/J$ in Eq. (7) is solely tuned to improve solution convergence. Above rated wind speed, a proportional-integral (PI) controller modifies the pitch to maintain the rated rotor speed.

2.3 Reference wind speed and normalization of quantities

We introduce the following decomposition of the mean flow:

$$u = U + u', \tag{8}$$

where u is the flow field including the turbine interacting with it, U is the undisturbed flow field, and u' quantifies the disturbance by the turbine. The reference wind speed employed throughout this work is the undisturbed rotor-equivalent wind speed (Wagner et al., 2011) calculated as

$$U_{\mathrm{Ref}} = \sqrt[3]{\frac{1}{A_{\mathrm{R}}} \int\limits_{A_{\mathrm{R}}} U_R^3 dA}, \tag{9}$$

with U_R being the undisturbed rotor-normal velocity component at the location of the rotor. This approach takes the variation of available kinetic energy over the rotor plane into account, and allows for a more accurate assessment of the efficiency of a turbine. However, it does not consider the streamwise development of the undisturbed flow field.

At every turbine location, U_{Ref} is obtained separately~~, thus~~ quantities like λ, C_P, and the axial induction a are normalized by the respective local U_{Ref} evaluated when the turbine is turned off ~~and not~~ by an upstream velocity.

2.4 Domain and grid design

The shape of the quasi-two-dimensional Gaussian hill is described by

$$h = h_0 \exp\left(-\frac{x^2}{2\sigma^2}\right) \tag{10}$$

and has in its standard configuration a height h_0 of 1 D and a standard width σ of 1.5 D with D denoting the turbine diameter. When the turbine is located ahead/at the foot of the hill (**B**), it is 4.5 D away from the top of the hill. The surface roughness is 0.001 m, which corresponds to a snowy surface ~~in reality~~ (Troen and Petersen, 1989). Three additional sets of simulations ~~of~~ the turbine on top of the hill are performed. In one case, the surface roughness is changed to 0.1 m, in the next one, the hill height is varied while the width is kept constant, and in the last case, the ratio between hill height and width is kept constant, while the height is varied. An overview of all simulations is listed in Tab. 1. The simulations are performed in two steps: First, the domain is simulated without the turbine to extract the undisturbed U_{Ref} at the turbine position. Second, after convergence of the empty domain, the turbine is switched on, and the simulation converged again to extract ~~power, induction, etc.~~

Table 1. Conducted simulations within this study. The controller is tuned based on optimal operation obtained from **A0**.

Label	Location	Hill height h_0 [D]	Hill width σ [D]	Surface roughnes z_0 [m]	Control/type of simulation
A0	Flat	0	-	0.001	C_P-λ-θ surface, no control
B0	Foot of hill	1	1.5	0.001	C_P-λ-θ surface, no control
C0	Top of hill	1	1.5	0.001	C_P-λ-θ surface, no control
A1	Flat	0	0	0.001	Controller
B1	Foot of hill	1	1.5	0.001	Controller
C1	Top of hill	1	1.5	0.001	Controller
C2	Top of hill	1	1.5	0.1	Controller
C3.1	Top of hill	0.75	1.5	0.001	Controller
C3.2	Top of hill	0.50	1.5	0.001	Controller
C3.3	Top of hill	0.25	1.5	0.001	Controller
C4.1	Top of hill	0.75	1.125	0.001	Controller
C4.2	Top of hill	0.50	0.75	0.001	Controller
C4.3	Top of hill	0.25	0.375	0.001	Controller
C4.4	Top of hill	0.125	0.1875	0.001	Controller

The computational domain is in all cases a curvilinear grid with a size of 45 × 18 × 34 D^3 in the x, y and z direction, respectively, which correspond to the streamwise, lateral and vertical dimension. The hill is generated by deforming the bottom surface of a flat domain. In total, the grid has a size of $256 \times 192 \times 192 = 9437184$ cells. In the turbine region, the mesh is refined with nearly cubic cells with a side length of 5 m, corresponding to a resolution of nearly 36 cells per D.

The turbine is simulated as an actuator disk, which is represented in the flow domain by a polar grid, and forces are projected onto the computational grid by the actuator shape approach (Réthoré et al., 2014; Troldborg et al., 2015). The tip-loss correction by Glauert is applied and the disk grid has 17 radial points and 64 azimuthal points.

For the case with the turbine located on the hill ridge, a sensitivity study the domain size has been performed by Zengler et al. (2024) showing a variation of the disk-averaged velocity for a fixed C_T of less than 0.1 % when increasing the cross-sectional area of the domain by a factor of eight. A sensitivity analysis of the cell size is carried out in this work, showing that U_{Ref} varies by less than 0.01 % when increasing the cell volume by a factor of eight. When the turbine is operating with a controller, the induction and power between these two different cell volumes vary by less than 2 %.

2.5 Turbulence model, inflow, boundary conditions and solver

The simulations are performed as RANS simulations using the k-ε-fp model (van der Laan et al., 2015b) as closure model. The standard model coefficients are left unaltered and the inflow is described by the analytical log-law solutions for the velocity

https://doi.org/10.5194/wes-2025-258
Preprint. Discussion started: 25 November 2025

U, the turbulence kinetic energy k and the dissipation ε (van der Laan et al., 2015a)

$$U = \frac{u_*}{\kappa} \log\left(\frac{z+z_0}{z_0}\right), \quad k = \frac{u_*^2}{\sqrt{C_\mu}}, \quad \varepsilon = \frac{u_*^3}{\kappa(z+z_0)}, \tag{11}$$

with the friction velocity u_* and the von-Kármán constant κ. It is important to mention that the level of turbulence intensity is independent of the friction velocity, which is varied in order to change the hubheight velocity.

The described inflow is set as a boundary condition at the inlet and at the top of the domain in order to maintain the logarithmic profile in the absence of obstacles. At the outlet, a zero-velocity gradient condition is imposed, and at the bottom, a rough wall boundary condition as described by Sørensen et al. (2007) is used. The lateral boundaries are periodic.

EllipSys3D (Michelsen, 1992, 1994; Sørensen, 1995) is used to solve the incompressible Navier Stokes equation in finite-volume formulation in a procedure similar to the SIMPLE algorithm (Sørensen, 2018).

3 Results

The results are organized by first presenting the prescribed C_P-λ-θ surfaces obtained at the three ~~considered~~ locations and analyzing the differences in $C_{P,\max}$, λ_{opt}, and θ_{opt}. The controller constant k is set using the values of $C_{P,\max}$ and λ_{opt} obtained at the flat location (**A0**). ~~After this,~~ power curve calculations are performed at all three turbine positions ~~with~~ this controller, and control-relevant quantities like λ and induction factors are discussed in this context.

3.1 C_P-λ-θ surfaces

Figure 2 shows C_P as a function of the blade pitch angle and the tip-speed ratio ~~(~~**A0**, **B0**, **C0**~~)~~. The surfaces are obtained on a grid with $\Delta\lambda$ = 1 and $\Delta\theta$ = 1 deg, and the maxima are found by cubic spline interpolation. In addition, at the optimal pitch in flat terrain (- 1.8 deg), the C_P-λ curves for all locations are simulated with $\Delta\lambda$ = 0.5. These curves will be later shown in Fig. 3. On top of the hill, sufficient convergence could not be reached for cases of λ = 10 and θ = -5, -4 deg.

In flat terrain, the optimal C_P is 0.543 at a blade pitch angle of $\theta =$ -1.8 deg and a tip-speed ratio of 8.1. These values differ from the ones specified for the DTU 10 MW RWT Bak et al. ~~(~~2013), which can be mainly attributed to the well-known fact that the induction in the rotor plane is usually over-predicted in AD simulations (Mikkelsen, 2004; Zengler et al., 2025a). As a consequence, the power coefficient is higher, and the blades need to be pitched back more to account for the change of the local flow angle. When the turbine is located at the foot of the hill, the maximum power performance increases by 3.5 % accompanied by a decrease of optimal pitch (-2.1 deg) and an increase of the tip-speed ratio (8.3). At the top of the hill, the opposite is true. The maximum power coefficient decreases by 20.0% to a value of 0.437 together with an increase of pitch (-0.4 deg) and a decrease of the tip-speed ratio (7.2). The indicated undisturbed velocity contours in Fig. 2 show that the flow accelerates behind the turbine located at the foot of the hill, while it decelerates behind the turbine at the hill top. In line with previous research (Revaz and Porté-Agel, 2024; Troldborg et al., 2022; Dar et al., 2023), deceleration results in a decrease in power performance while acceleration results in an increase. The presented C_P surfaces indicate that there is no possibility of operating at the same optimal power coefficient as in the flat case when the turbine is operating on the hill, regardless of pitch

https://doi.org/10.5194/wes-2025-258
Preprint. Discussion started: 25 November 2025

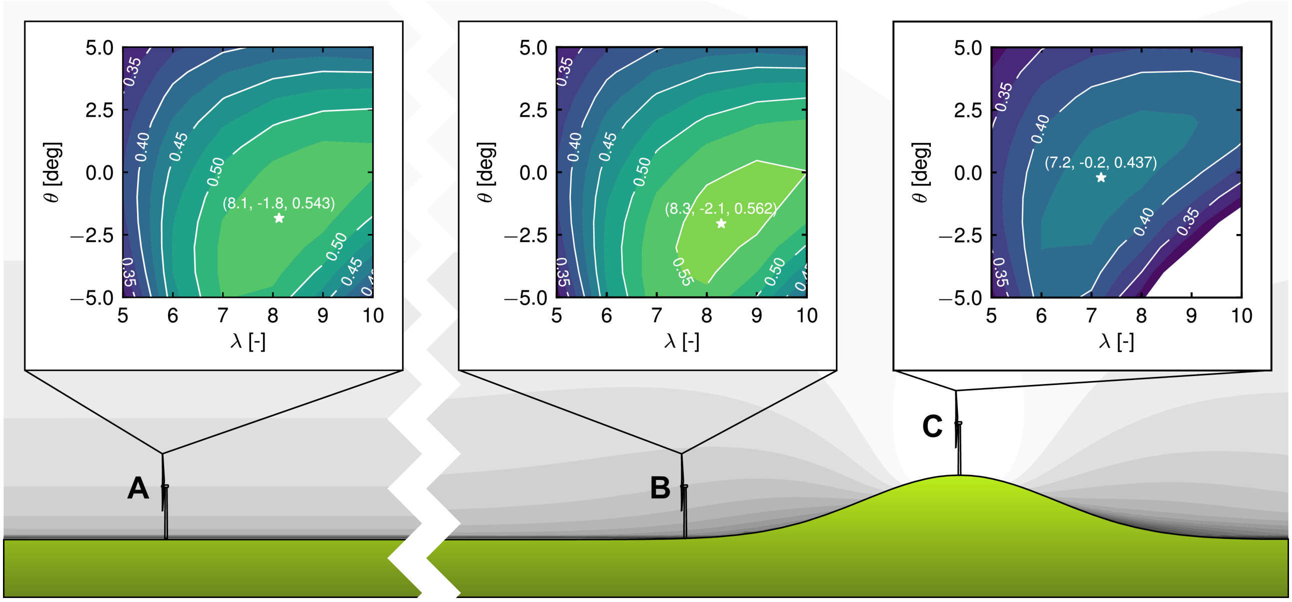

Figure 2. C_P surfaces obtained in a flat domain (**A0**, left), on the foot of the hill (**B0**, center) and on top of the hill (**C0**, right). White stars indicate the point of optimal power performance. Iso-curves of the undisturbed flow velocity magnitude in the graphic illustrate regions of speed-up in the vicinity of the hill.

and tip-speed ratio, because the available power is limited by the flow development. However, this does not necessarily mean that placing a turbine on top of a hill leads to worse power performance in absolute numbers, because wind speeds on top of hills are often higher. The actual benefit one can expect by placing a wind turbine on a hill will be discussed in Sec. 4.3.

3.2 Simulations with active controller

The pitch and torque controllers are tuned based on the steady-state optimal performance in flat terrain (**A0**). The torque constant (Eq. 6) is set to $k = 11 \times 10^6$ Nms^2 and the rated generator speed is set to 1.0 rad^{-1}. The minimum pitch the pitch controller can operate at is set to -1.8 deg. Because the pitch controller is a PI controller that tracks the error between generator speed and rated generator speed, the negative error below rated wind speed will result in a negative pitch signal, which will saturate at this minimum pitch of -1.8 deg. As a consequence, in region two, the pitch is held constant at -1.8 deg, which can also be seen in Fig. 1 ~~(b)~~. With the calibrated controller, the power curves are run for an increasing wind speed, which is achieved by varying the friction velocity u_* in Eq. (11).

The key simulation results at the three positions are shown in Fig. 3 (a). All power curves show the three typical distinct regions in which a turbine operates: region ~~one,~~ below cut-in wind speed, where no energy is produced, region ~~two,~~ where the primary objective is the maximization of energy production, and region ~~three,~~ where energy extraction is limited to the rated power. The turbine on top of the hill produces significantly less energy below rated wind speed than the one in flat terrain for the same undisturbed ~~rotor~~ wind speed at the rotor, while the one at the hill's foot produces slightly more energy for the same

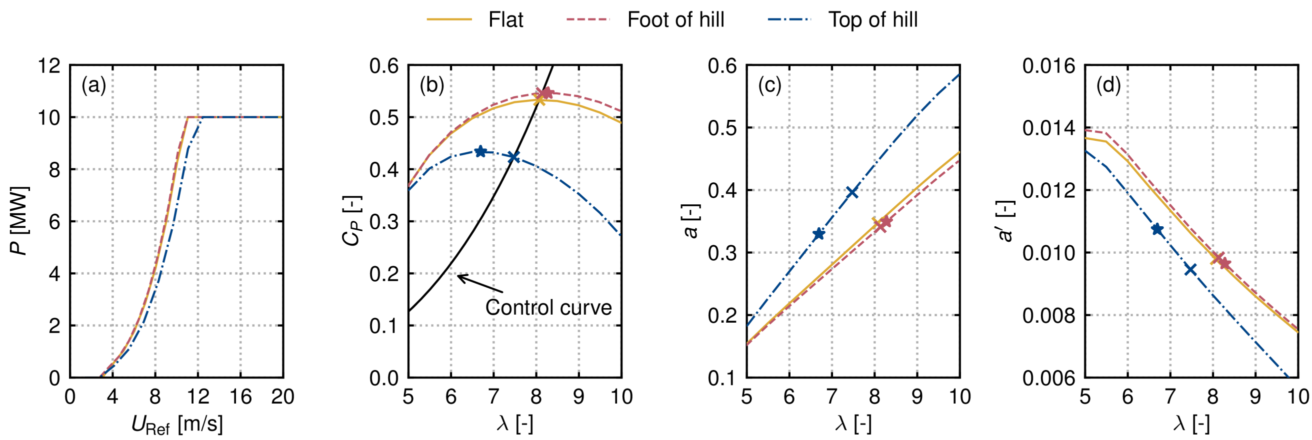

Figure 3. Simulation results for the controlled turbine placed at the three different positions (**A1**, **B1**,**C1**): (a) Power curves, (b) C_P-λ curves with control curve in solid black, steady state operational points below rated wind speed marked as crosses and maximum C_P marked by stars, (c) induction curves and operational points with $a = 1 - u_R/U_{\text{Ref}}$ where u_R is the kinetic energy mean over the rotor calculated like U_{Ref} in Eq. (9) and (d) tangential induction $a' = u_{R,t}/(\omega r)$ evaluated as azimuthal mean at $r = 0.75R$.

undisturbed rotor wind speed. Note that although the wind speed changes, Reynolds-similarity leads to the development of similar flow features independent of the wind speed (van der Laan et al., 2020), which is why the induction below rated wind speed is unaltered by the inflow velocity. Above rated conditions, all turbines produce the same power as a consequence of the pitch controller aiming ~~at maintaining~~ a certain rotor speed independently of the energy content of the flow. Although this work does not focus on region 2.5, one can see that its onset is delayed for the turbine on the hilltop due to a lower rotational speed for a given undisturbed rotor wind speed.

Figure 3 (b) shows the C_P-λ curve, including the points where the torque controller settles in region ~~two~~ during the power curve calculation. Regardless of the turbine position, the controller settles at the intersections ~~between~~ the control curve given by Eq. (4) and the respective performance curves. ~~Especially from~~ the case ~~on top of the hill,~~ it becomes apparent that this intersection does not necessarily represent the point of maximum power capture. In numbers, at the foot of the hill, the turbine produces 2.4% more power than in flat terrain with the same undisturbed reference wind speed, while it produces 20.6% less power on top of the hill.

Figure 3 (c) shows the axial induction as a function of λ. At the foot of the hill, it is always lower than in flat terrain, while on top of the hill, it is always higher, corresponding to a higher and lower C_P, respectively. It is observed that at the top of the hill, the optimal tip-speed ratio would be approximately 6.7, resulting in a ~~decreasing~~ induction relative to the flat case. On the other side, the controller settles at a tip speed ratio of 7.5 with an increased induction relative to the flat case.

In Fig. 3 (d), the azimuthally averaged tangential induction evaluated at 0.75 R is presented. The a'-λ curves show an opposite trend to the a-λ curves. The tangential induction in general decreases with an increasing tip-speed ratio; however, for a given tip-speed ratio, it is always lower at the top of the hill and higher ahead of the hill, so following the opposite trend compared to the axial induction. In comparison to the axial induction, the tangential induction of the controlled cases (marked by crosses) seems to stay rather constant during operation at the three different locations. Only a small trend can be observed: Ahead of the hill, the tangential induction increases, while it decreases on top of the hill. In Sec. 4.1, it will be discussed whether tangential induction is expected to stay constant during torque control. There, the radial distributions of axial and tangential induction will also be shown.

4 Discussion

The previous section showed that the power performance is markedly affected when a flat-terrain-designed turbine operates under complex-terrain conditions. This is primarily a consequence of the flow physics as seen in Fig. 2. Additionally, the controller leads to suboptimal performance in these situations as seen in Fig. 3 (b).

Next, we characterize the behavior of the torque and pitch controllers. It is ~~furthermore~~ asked how strong the deterioration of the actual power is, considering the effect of higher wind speeds on top of the hill relative to flat terrain. Lastly, the limitations of the present study are discussed.

4.1 Role of torque controller

Figure 3 ~~(b)~~ shows that the torque controller follows its prescribed control curve as expected, even when the surrounding flow field changes to conditions the controller was not calibrated for. On the one side, this is not surprising, because eventually ~~a~~ torque controller enforces

$$\frac{C_{P,\max}}{\lambda_{\mathrm{opt}}^3} = \frac{C_P}{\lambda^3} \tag{12}$$

for any operational state (as seen in Eq. (4)) with the left-hand side being constant and calibrated, for example, for flat terrain in our case. On the other hand, this relation does not directly yield insights into how a or the local a' change due to the effect of complex terrain.

4.1.1 Impact on performance coefficients

We formulate the torque control strategy based on the velocity at the disk during operation. For this purpose, we introduce the operational power coefficient, thrust coefficient, and tip-speed ratio as

$$C_P^* = \frac{P}{\frac{1}{2}\rho u_D^3 A} = C_P \left(\frac{U_{\mathrm{Ref}}}{u_D}\right)^3, \tag{13}$$

$$C_T^* = \frac{T}{\frac{1}{2}\rho u_D^2 A} = C_T \left(\frac{U_{\mathrm{Ref}}}{u_D}\right)^2, \tag{14}$$

$$\lambda_* = \frac{\omega R}{u_D} = \lambda \frac{U_{\mathrm{Ref}}}{u_D}, \tag{15}$$

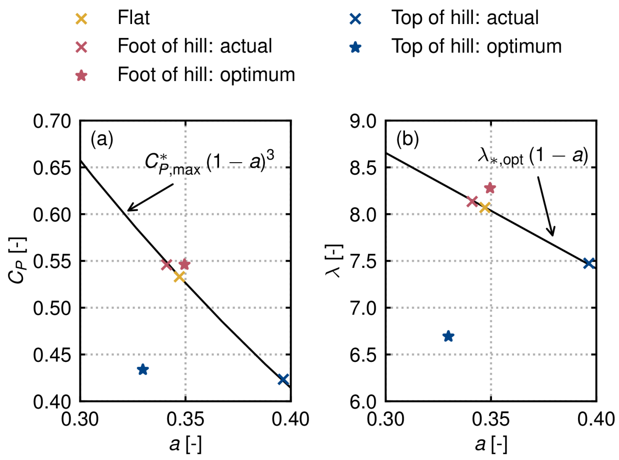

Figure 4. Power coefficient and tip-speed ratio as a function of the induction in flat terrain, ahead of the hill and on top of it together with Eq. (19) and Eq. (21) and the points of optimal operation at every position.

where u_D is the flow in the turbine plane during operation, calculated similarly to Eq. (9). The optimal power operation is then reformulated as

$$P_{\max} = \frac{1}{2}\rho\pi R^2 C^*_{P,\max} u_D^3 = \underbrace{\frac{1}{2}\rho\pi R^5 \frac{C^*_{P,\max}}{\lambda^3_{*,\mathrm{opt}}}}_{k}\,\omega^3 \tag{16}$$

This shows that optimal control actually enforces an equilibrium between power and the velocity in the turbine plane during operation, independently of the free-stream velocity. This makes intuitive sense because eventually the forces and moments on the turbine blades purely depend on what the local flow is at the disk. In fact, the only thing that a torque controller keeps constant is the ratio between torque and rotor speed squared, regardless of what velocity is used as reference velocity as seen in Eq (4). Because rotor speed and disk velocity are related by a constant during torque control in order to keep the local flow angles constant, an equilibrium between power and disk velocity during operation is also achieved (Zengler et al., 2025b). Thus, a turbine calibrated for a certain operational point keeps C_P^* constant and not C_P. In our simulations, we find that C_P^* and λ_* are practically constant; $C^*_{P,\max} = 1.92 \pm 0.0076$ and $\lambda_{*,\mathrm{opt}} = 12.36 \pm 0.016$.

The introduction of certain non-dimensional quantities hides the actual physics happening here. The relation between C_T and a changes in terrain, but not the relation between the local blade forces and velocities. To circumvent this problem, one could either use quantities for non-dimensionalization that do not change, such as u_D in our case, or work exclusively in dimensional form. This, on the other hand, would make it difficult to compare results.

Returning to torque control, for the optimal thrust, it follows that

$$T_{\mathrm{opt}} = \frac{1}{2}\rho\pi R^2 C^*_{T,\mathrm{opt}} u_D^2 = \underbrace{\frac{1}{2}\rho\pi R^4 \frac{C^*_{T,\mathrm{opt}}}{\lambda^2_{*,\mathrm{opt}}}}_{\text{constant}}\,\omega^2, \tag{17}$$

from which ~~it~~ can be ~~furthermore~~ deducted that

$$\frac{C_T}{\lambda^2} = \frac{C_T^*}{\lambda_*^2} = \text{constant}. \tag{18}$$

How do these considerations now affect a, a', C_P and C_T during torque control? Based on Eqs. (13), (14), and (15) the following relations are obtained

$$C_P = C_{P,\max}^* \left(1-a\right)^3, \tag{19}$$

$$C_T = C_{T,\mathrm{opt}}^* \left(1-a\right)^2, \tag{20}$$

$$\lambda = \lambda_{*,\mathrm{opt}} \left(1-a\right). \tag{21}$$

In Fig. 4, Eqs. (19) and (21) are shown alongside the simulation results showing that indeed the turbine always operates on these curves. At this point, it is worth taking a look at control strategies, which set blade forces based on u_D and C_T^* (van der Laan et al., 2014; Meyers and Meneveau, 2010; Calaf et al., 2010). The current findings show that classical torque control is equivalent to these strategies, keeping C_T^* and C_P^* constant, rather than C_T and C_P. This has also been shown ~~before~~ (Zengler et al., 2025b).

4.1.2 Impact on tangential induction

The question of why the tangential induction a' shown in Fig. 3 (d) seems to be independent of the effects of the complex terrain, when the other quantities are affected by it, is so far unanswered. In order to answer this, a local analysis of the blade forces is carried out in appendix A. By considering only the effect of lift forces on the flow and neglecting drag, it can be shown that a' can be calculated as

$$a'(\mu) = \frac{1}{2}\left(-1 + \sqrt{1 + \frac{C_t(\mu)}{\lambda^2 \mu^2}}\right), \tag{22}$$

with the non-dimensional radial coordinate $\mu = r/R$ and the local thrust coefficient C_t. From this equation, it is evident that a' only depends on the local blade forces and rotor speed. The reference velocity used for normalization of λ and C_t can be omitted from the equation, because C_t is normalized by U_{Ref}^2 and λ by U_{Ref}, so when dividing C_t by λ^2, U_{Ref} cancels out. It was shown in Eq. (18) that the ratio $\frac{C_T}{\lambda^2}$ is constant for a torque controller. Based on this, it can therefore be argued that the local version of that ratio $\frac{C_t(\mu)}{\lambda^2}$ should be constant as well, as long as changes in the flow state due to terrain are uniform over the disk. This explains why a' is independent of the effects of complex terrain in region two, although rotor speed and thrust change; it is simply a consequence of the torque control. In Fig. 5 (a) and (b), the local axial and tangential inductions are shown as function of radial position along the blade as well as the angle of attack α in (c). Indeed, the tangential induction is nearly identical in all cases. Only close to the root are deviations between the cases visible. A possible explanation for this is that in this region drag plays a significant role, also affecting the tangential induction.

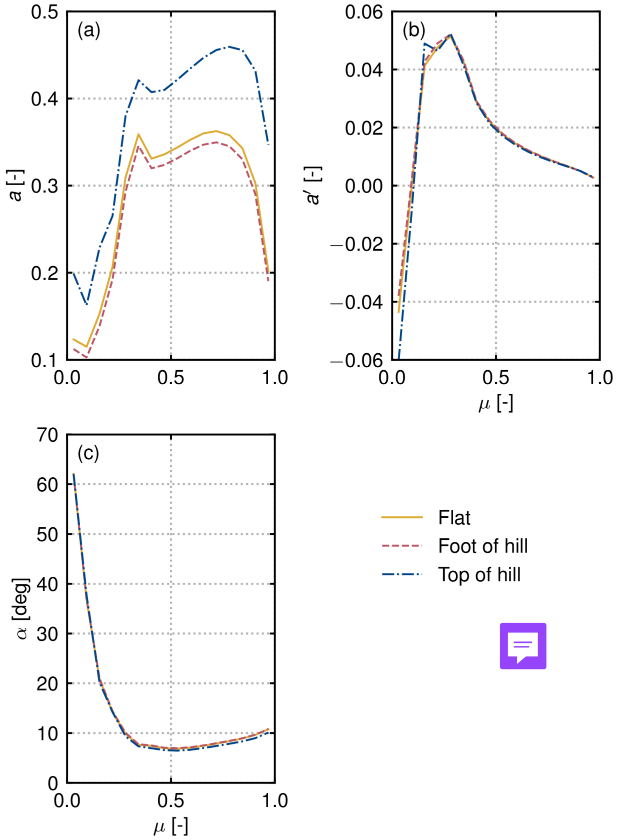

Figure 5. Azimuthally averaged axial induction (a), tangential induction (b), and angle of attack α (c) shown as a function of nondimensional radial position $\mu = r/R$.

4.1.3 Optimal performance

We briefly discuss how a controller would need to operate to always track optimal performance. From Eq. (21), one can see that the rotor speed (λ) decreases with a decreasing disk velocity (an increasing induction a). In Fig. 4 (b), the optimal performance on top of the hill would be reached by reducing the induction and also reducing the tip-speed ratio. From a local perspective, this results in higher axial velocities and lower relative tangential velocities. As a consequence, the local flow angle and angle of attack increase when not adjusting pitch. However, as suggested by Fig. 2, also the pitch should be modified to track optimal performance, which would eventually change the angle of attack.

Ahead of the hill, when the background flow is accelerating, the opposite is the case; to track optimal performance, the angle of attack would need to decrease. This observation is also in agreement with previous findings based on momentum theory (Zengler et al. (2025a), see also Eq. (B5)), which show that in a decelerating flow, the optimal performance would be reached at a lower induction, while in an accelerating flow, it would be reached at a higher induction. Without modification of the torque

https://doi.org/10.5194/wes-2025-258
Preprint. Discussion started: 25 November 2025

constant, a torque controller would therefore always operate below optimum in accelerating flow fields, because it effectively keeps flow angles constant instead of adjusting them to the flow conditions. Since blades are often designed to achieve the best two-dimensional polar lift-to-drag ratios at the angles of attack corresponding to region ~~two~~ operation, torque control ensures that the airfoil sections are performing well from a two-dimensional perspective. The reason for suboptimal power performance is the changed (axial) induction response in accelerating flows.

A way of approaching this problem of suboptimal power performance outside the flat operating conditions would be to include control algorithms, which slowly modify the torque constant (and pitch) over time to reach optimal performance (see for example extremum seeking control, Creaby et al. (200[illegible])). However, as Fig. 3 (b) indicates, the total gain in performance is rather low on a given curve. Also, the gradient $\frac{\partial C_P}{\partial \lambda}$ might not be very strong. In combination with varying atmospheric conditions, which are not part of this study, and also seasonal variations of the terrain, optimization of the torque constant might be difficult and the expected gain possibly small, if not even negligible.

In summary, a torque controller enforces C_P^*, C_T^*, and λ_* to stay constant. A consequence is that also a' is constant, which only depends on the local forces and flow. Because of the changing optimal inflow angles in complex terrain, a torque controller cannot operate optimally with this strategy.

4.2 Role of the pitch controller in region ~~two~~

The pitch controller tracks the difference between the actual and rated rotor speed. In region ~~three~~ of the power curve, this leads to the observed behavior that even in a non-uniform background flow, the same rated power is reached in the different cases. In region ~~two,~~ the pitch controller remains inactive, although Fig. 2 suggests that performance could be increased by adjusting the pitch. The reason for this is the implementation of the pitch controller as a PI controller. Below the rated wind speed, or rather the rated rotor speed, the difference between actual and rated rotor speed is negative, resulting in a negative pitch signal saturating at the minimum pitch independently of the flow state. Similarly to the torque controller, one could imagine an algorithm that modifies the minimum pitch seeking maximum power performance in region 2 of the power curve. However, in practice, it might again be difficult because of the small differences between optimal and actual pitch.

4.3 Speed-up factors

A common way to account for the effect of complex terrain is to use speed-up factors. Because power scales with the wind speed cubed in the flat terrain case, the effect of terrain on the power of a turbine is usually estimated as

$$P_{\text{hill}} \approx P_{\text{flat}}(1+\Delta U)^3, \tag{23}$$

with $\Delta U = (U_{\text{Ref,hill}} - U_{\text{Ref,flat}})/U_{\text{Ref,flat}}$ being a non-dimensional velocity speed-up factor. This estimate is only accurate as long as the actual power coefficient of the turbine is the same as that in the flat terrain case. However, as shown before, when the turbine is located on a hill, the power coefficient decreases due to the streamwise development of the flow behind the turbine. This raises the question of what is actually the maximum performance that can be reached by placing wind turbines on elevated spots, such as hills.

https://doi.org/10.5194/wes-2025-258
Preprint. Discussion started: 25 November 2025

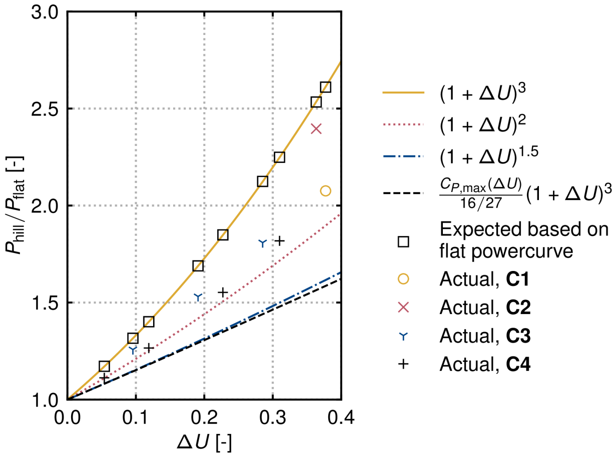

Figure 6. Expected and actual power at the top of the hill for different speed-up factors. The variation in speed-up is reached by changing the roughness to 0.1 m (**C2**), varying the hill height and keeping the width constant (**C3.1**-**C3.3**), and by varying the hill height while keeping the ratio between width to height constant (**C4.1**-**C4.4**). The turbines were simulated, including a controller, so the potential maximum power performance would be around one percent higher.

To answer this question, we consult the additional simulations mentioned at the beginning (**C2**, **C3.1**-**C3.3**, **C4.1**-**C4.4**) and use a model that incorporates the effect of streamwise velocity gradients on the power coefficient (Zengler et al., 2025a). By assuming that the maximum deceleration behind the hill is similar to the speed-up ahead of the hill and that the speed-up region is smaller than the region where the wake pressure equalizes with the surrounding pressure, the change of the maximum power coefficient as a function of the speed-up ΔU, i.e. $C_{P,\max}(\Delta U)$, according to this model can be estimated, which is outlined in appendix B in more detail. Because this model yields identical results to momentum theory for $\Delta U = 0$, the scaling of the power on a hill can be estimated to be

$$P_{\text{hill}} = P_{\text{flat}} \frac{C_{P,\max}(\Delta U)}{16/27}(1+\Delta U)^3, \tag{24}$$

$$\approx P_{\text{flat}}(1+\Delta U)^{1.5}, \tag{25}$$

with the second line being an approximation based on visual inspection of the resulting curves. This estimate requires that the flow recovers to the flat terrain-state directly behind the turbine, and can therefore be interpreted as a lower bound to the possible maximum power performance. To investigate how the power changes on top of the hill in the simulations presented, the actual power increase is shown together with the traditional cubic trend (Eq. (23)), the lower bound from Eq. (24), its approximation (Eq. (25)), and a quadratic scaling for reference in Fig. 6. It is important to keep in mind that the simulation results also include a controller; thus, the actual maximum available power is expected to be around one percent higher, as shown in Fig. 3 (b).

https://doi.org/10.5194/wes-2025-258
Preprint. Discussion started: 25 November 2025

As expected, the actual power increase on top of the hill does not follow a cubic trend, but is in all cases lower. When the flow separates behind the hill, as is the case for $z_0 = 0.1$ m, and the velocity immediately behind the turbine does not decelerate so strongly, the power is closer to the cubic relationship. The same conclusions can be made comparing simulations **C3.1-C3.3** with **C4.1-C4.4**. When the width does not change, the deceleration behind the turbine is weaker, and the respective power performance is higher. Reducing both width and height results in a more local speed-up followed by a strong deceleration. None of the presented cases seems to scale according to Eq. (24), the scaling is always higher, rather than being close to a quadratic trend. Only for very small speed-ups, the scaling seems to approach the predictions. As outlined previously, this can be explained through the assumptions made for deriving Eq. (24), which requires a very local speed-up with immediate wake recovery. These observations suggest that if terrain and flow features in the vicinity of the turbine are more similar to flat terrain features, such as a very long hill or a separation bubble that delays deceleration, the maximum power coefficients are also similar, leading to a more cubic scaling of power. If this is not the case, and flow and terrain features vary on similar length scales as those of the turbine, a stronger influence on the power coefficient can be expected.

Based on this analysis, it is concluded that placing a wind turbine in a spot where the speed is locally highest is beneficial for power performance. However, the limitation of the free stream velocities in the wake region potentially reduces the achievable gain from what is expected from the classical cubic relation (Eq. (23)). In cases where turbines are located in smaller local free stream speed-up regions, the scaling exponent from the simulations was closer to 2, with even slower (but still positive) scaling indicated by Eq. (24) by theoretical means.

4.4 Limitations

Although this work deals with complex terrain, the studied case of a wind turbine on a quasi-two-dimensional Gaussian hill remains a significant simplification. The undisturbed flow field is quasi-two-dimensional and varies only in the vertical and streamwise direction. Furthermore, the effect of atmospheric stability was not included. It remains a subject for future studies how a three-dimensional, unsteady flow would interact with the wind turbine, and to what extent the result that optimal induction decreases in a decelerating flow and increases in an accelerating flow also holds there.

5 Conclusions

Wind turbine performance in complex terrain is affected by a streamwise non-uniform flow field, resulting in changing limits of maximal energy extraction and by the control algorithm, not capable of adjusting properly to the physics caused by the modified flow conditions. It was shown that a torque controller keeps thrust and power coefficient based on the disturbed flow field constant, which do not necessarily correspond to the point of operation, which yields maximum power performance in non-uniform flow fields. The present results suggest that a torque-based control would always lead to a ~~non-~~optimal power performance in accelerating flows, because the optimal local flow angles change, while a torque controller keeps the local flow angles constant. Whether including additional knowledge about the flow field in the control strategy and adjusting the torque constant and pitch is beneficial overall remains to be investigated. It was shown that placing turbines in elevated regions with higher wind speeds is beneficial for power performance. However, the degradation of the power coefficient leads to a reduced power output, not scaling with the speed-up over the hill cubed. The observed scaling in the simulations was closer to a quadratic trend, while theoretical considerations suggest a lower limit of the scaling close to the power of 1.5.

Code and data availability. EllipSys3D used for the simulations is a proprietary software developed at DTU Wind and Energy Systems and distributed under licence.

Appendix A: The effect of flow acceleration on the tangential induction

The simulation results show that the tangential induction is barely affected by the acceleration of the background flow, and major differences between the simulations can only be observed close to the root. At the root, the energy conversion process is different compared to the blade tips, because structural constraints require thick airfoils with a low lift-to-drag ratio, resulting in a flow that is significantly influenced by the drag of the airfoil. With this knowledge in mind, we now seek to investigate why the tangential induction is rather independent of flow acceleration in the outer region of the blade.

A control volume analysis of the conservation of angular momentum yields (Hansen, 2015)

$$dQ = r\,u_t^+\,d\dot{m} = 4\pi\rho R^2\mu^3\lambda U_{\mathrm{Ref}}^2(1-a)a'\,dr, \tag{A1}$$

with u_t^+ being the tangential velocity in the wake, which relates to the tangential induction as $a' = u_t^+/(2\omega r)$. Further we used for the mass flux $d\dot{m} = U_{\mathrm{Ref}}(1-a)2\pi r\,dr$. Note that $U_{\mathrm{Ref}}(1-a)$ only describes the velocity in the rotor plane, independently of what caused this velocity. Shifting the view towards the blade, the angular momentum can be calculated as

$$dQ = f_t N_B r\,dr, \tag{A2}$$

with the tangential force per spanlength f_t and the number of blades N_B. When taking a look at the force and flow vectors at each blade section, we now consciously ignore the drag of the airfoil yielding for the flow angle ϕ

$$\tan\phi = \frac{U_{\mathrm{Ref}}(1-a)}{\omega r(1+a')} = \frac{f_t}{f_n}, \tag{A3}$$

with the blade normal force per spanlength f_n. For the local thrust coefficient, we obtain

$$C_t = \frac{dT}{\frac{1}{2}\rho U_{\mathrm{Ref}}^2\,dA} = \frac{dT}{\pi\rho U_{\mathrm{Ref}}^2 r\,dr} = \frac{f_n N_B}{\pi\rho U_{\mathrm{Ref}}^2 r}. \tag{A4}$$

Combining Eq. (A3) with Eq. (A4) yields for the tangential force

$$f_t = \frac{1-a}{1+a'}\frac{\pi R\rho U_{\mathrm{Ref}}^2 C_t}{\lambda N_B}, \tag{A5}$$

and by combining this with Eq. (A1) and Eq. (A2), we obtain

$$a'(1+a') = \frac{C_t}{4\lambda^2\mu^2}, \tag{A6}$$

which can be solved for the tangential induction yielding Eq. (22), showing that indeed, in regions where lift dominates the flow, the tangential induction only depends on $\frac{C_t}{\lambda^2}$, which a torque controller keeps constant.

The same result can be obtained in a vortex-theory framework without the need for a control-volume analysis, which is briefly outlined below. For an actuator disk with azimuthal constant loading, the induced tangential velocity due to the bound vortex of strength Γ_B can be calculated from the definition of circulation Γ as

$$\Gamma = \oint u_s \, ds = 2\pi r u^+_{t,i} = N_B \Gamma_B \tag{A7}$$

with u_s being the tangential velocity along the curve s and $u^+_{t,i}$ being the mean induced velocity behind the disk. Ahead of turbine, the mean induced velocity is $u^-_{t,i} = 0$ and therefore in the disk plane the induced velocity is

$$u_{t,i} = \frac{1}{2}\left(u^-_{t,i} + u^+_{t,i}\right) = \frac{N_B \Gamma_B}{4\pi r}. \tag{A8}$$

Based on the Kutta-Joukowsky condition, the axial force per spanlength is calculated as $f_n = \rho \Gamma_B u_t$, yielding for the local C_t previously defined in Eq. (A4)

$$C_t = \frac{\Gamma_B u_t N_B}{U^2_{\mathrm{Ref}} \pi r}. \tag{A9}$$

The total local tangential velocity relative to the blades can be calculated as the sum of the rotational component and the induced velocity

$$u_t = U_{\mathrm{Ref}} \lambda \mu + u_{t,i}. \tag{A10}$$

Using Eq. (A8) and introducing the non-dimensional bound circulation $\gamma = \frac{\omega N_B \Gamma_B}{\pi U^2_{\mathrm{Ref}}}$ yields

$$u_t = U_{\mathrm{Ref}} \lambda \mu \left(1 + a'\right), \tag{A11}$$

with the tangential induction defined as

$$a' = \frac{\gamma}{4\lambda^2 \mu^2}. \tag{A12}$$

Inserting this into Eq. (A9) yields

$$C_t = 4a' \lambda^2 \mu^2 \left(1 + a'\right), \tag{A13}$$

which is identical to the result from the momentum analysis Eq. (A6).

Appendix B: Change of maximum C_P on an isolated hill

Zengler et al. (2025a) developed an engineering model based on momentum theory, which incorporates the effect of a streamwise acceleration of the background flow field. The modified equation for the power coefficient is

$$C_P = 4a(1-a)^2 + 4a(1-a)l\beta, \tag{B1}$$

with the term $l\beta$ being the product of a non-dimensional length scale l and a non-dimensional streamwise velocity gradient $\beta = \frac{D}{U_{\mathrm{Ref}}}\frac{dU}{dx}$. The length scale was assumed to be the distance behind the turbine, where the pressure in the wake equalizes with the surrounding pressure. It is often assumed that this point is around one diameter behind the turbine (Crespo et al., 1999; Dar and Porté-Agel, 2022), although research shows that its actual position depends on the thrust coefficient of the turbine and might be longer than one diameter (Liew et al., 2024). The undisturbed velocity behind the turbine where the background pressure equalizes is consequently

$$U_1 = U_{\mathrm{Ref}}(1 + l\beta). \tag{B2}$$

Now we consider a turbine located on a small hill. The speed-up ΔU over the hill is assumed to occur over a distance smaller than the distance over which the pressures in the wake of the turbine equalize. So we are speaking of a very local speed-up close to the turbine. As a consequence, the velocity U_1, at which the pressures equalize, is limited by this speed-up or rather speed-down behind the hill. With the notation introduced in the discussion of the speed-up factors in Sec. 4.3 with $U_{\mathrm{Ref,hill}}$ being the undisturbed velocity on top of the hill and $U_{\mathrm{Ref,flat}}$ being the undisturbed velocity around the hill, this means that $U_1 = U_{\mathrm{Ref,flat}}$. Expressing it in terms of the velocity on top of the hill, where the turbine is located yields

$$U_1 = U_{\mathrm{Ref,hill}}\left(1 - \frac{\Delta U}{1 + \Delta U}\right). \tag{B3}$$

Comparing this expression with Eq. (B2), we see that

$$l\beta = -\frac{\Delta U}{1 + \Delta U}. \tag{B4}$$

Next, we ask what the optimal performance a turbine can achieve is based on these considerations. Keeping the $l\beta$-notation for the sake of brevity, the induction, which maximizes C_P is found by differentiation of Eq. (B1) to be

$$a_{\mathrm{opt}} = \frac{2}{3} + \frac{1}{3}l\beta - \frac{1}{3}\sqrt{1 + l\beta + l^2\beta^2}. \tag{B5}$$

For $l\beta = 0$, one obaines $a_{\mathrm{opt}} = \frac{1}{3}$, which is the classical result from momentum theory. $C_{P,\mathrm{max}}$ can be determined by inserting the optimal induction into the equation for the power coefficient (B1). This result is, based on the previous argument, only valid for the case, where the undisturbed velocity behind the turbine immediately recovers to the velocity around the hill before the pressure equalizes with the surrounding flow.

Author contributions. CPZ: conceptualization, data curation, formal analysis, investigation, methodology, visualization, writing (original draft preparation) MG: conceptualization, methodology, formal analysis, supervision, writing (review and editing) NT: conceptualization, methodology, supervision, writing (review and editing)

Competing interests. The contact author has declared that none of the authors has any competing interests.

Acknowledgements. This work has been partially supported by the EU project MERIDIONAL with grant agreement No. 101084216. We also gratefully acknowledge the computational and data resources provided on the Sophia HPC Cluster at the Technical University of Denmark (https://doi.org/10.57940/FAFC-6M81).

References

Abbas, N. J., Zalkind, D. S., Pao, L., and Wright, A.: A reference open-source controller for fixed and floating offshore wind turbines, Wind Energy Science, 7, 53–73, https://doi.org/10.5194/wes-7-53-2022, 2022.

Bak, C., Zahle, F., Bitsche, R., KIm, T., Yde, A., Henriksen, L. C., Natarajan, A., and Hansen, M. H.: Description of the DTU 10 MW Reference Wind Turbine, Tech. Rep. DTU Wind Energy Report-I-0092, DTU Wind Energy, Roskilde, Denmark, 2013.

Bianchi, F. D., Mantz, R. J., and Battista, H. d., eds.: Wind Turbine Control Systems: Principles, Modelling and Gain Scheduling Design, Advances in Industrial Control, Springer London, London, ISBN 978-1-84628-492-2 978-1-84628-493-9, https://doi.org/10.1007/1-84628-493-7, 2007.

Bossanyi, E. A.: The Design of closed loop controllers for wind turbines, Wind Energy, 3, 149–163, https://doi.org/10.1002/we.34, publisher: Wiley, 2000.

Cai, T., Cheng, S., Segalini, A., and Chamorro, L. P.: Local topography-induced pressure gradient effects on the wake and power output of a model wind turbine, Theoretical and Applied Mechanics Letters, 11, 100 297, https://doi.org/10.1016/j.taml.2021.100297, 2021.

Calaf, M., Meneveau, C., and Meyers, J.: Large eddy simulation study of fully developed wind-turbine array boundary layers, Physics of Fluids, 22, 015 110, https://doi.org/10.1063/1.3291077, 2010.

Creaby, J., Li, Y., and Seem, J. E.: Maximizing Wind Turbine Energy Capture Using Multivariable Extremum Seeking Control, Wind Engineering, 33, 361–387, https://doi.org/10.1260/030952409789685753, publisher: SAGE Publications, 2009.

Crespo, A., Hernández, J., and Frandsen, S.: Survey of Modelling Methods for Wind Turbine Wakes and Wind Farms, Wind Energy, 2, 1–24, https://doi.org/10.1002/(SICI)1099-1824(199901/03)2:1<1::AID-WE16>3.0.CO;2-7, 1999.

Dar, A. S. and Porté-Agel, F.: An Analytical Model for Wind Turbine Wakes under Pressure Gradient, Energies, 2022, 5345, https://doi.org/10.3390/en15155345, 2022.

Dar, A. S., Gertler, A. S., and Porté-Agel, F.: An experimental and analytical study of wind turbine wakes under pressure gradient, Physics of Fluids, 35, 045 140, https://doi.org/10.1063/5.0145043, 2023.

Dar, A. S., Revaz, T., and Porté-Agel, F.: A model for the effect of pressure gradient on the induction and power of wind turbines, Physics of Fluids, 37, 085 128, https://doi.org/10.1063/5.0277577, publisher: AIP Publishing, 2025.

Hansen, M. O. L.: Aerodynamics of wind turbines, Routledge, London, New York, 3 edn., ISBN 978-1-138-77507-7, 2015.

Jonkman, J., Butterfield, S., Musial, W., and Scott, G.: Definition of a 5-MW Reference Wind Turbine for Offshore System Development, Tech. Rep. NREL/TP-500-38060, 947422, National Renewable Energy Laboratory, https://doi.org/10.2172/947422, 2009.

Liew, J., Heck, K. S., and Howland, M. F.: Unified momentum model for rotor aerodynamics across operating regimes, Nature Communications, 15, 6658, https://doi.org/10.1038/s41467-024-50756-5, 2024.

Liu, L. and Stevens, R. J. A. M.: Effects of Two-Dimensional Steep Hills on the Performance of Wind Turbines and Wind Farms, Boundary-Layer Meteorology, 176, 251–269, https://doi.org/10.5194/wes-7-1527-2022, 2020.

Meyers, J. and Meneveau, C.: Large Eddy Simulations of Large Wind-Turbine Arrays in the Atmospheric Boundary Layer, in: 48th AIAA Aerospace Sciences Meeting Including the New Horizons Forum and Aerospace Exposition, American Institute of Aeronautics and Astronautics, Orlando, Florida, ISBN 978-1-60086-959-4, https://doi.org/10.2514/6.2010-827, 2010.

Michelsen, J.: Basis3D - a Platform for Development of Multiblock PDE Solvers, Tech. rep., Technical University of Denmark, 1992.

Michelsen, J.: Block structured multigrid solution of 2D and 3D elliptic PDE's, Tech. rep., Technical University of Denmark, 1994.

Mikkelsen, R.: Actuator disc methods applied to wind turbines, Ph.D. thesis, Technical University of Denmark, Lyngby, Denmark, 2004.

Pao, L. Y. and Johnson, K. E.: Control of Wind Turbines, IEEE Control Systems, 31, 44–62, https://doi.org/10.1109/mcs.2010.939962, publisher: Institute of Electrical and Electronics Engineers (IEEE), 2011.

Revaz, T. and Porté-Agel, F.: Effect of hills on wind turbine flow and power efficiency: A large-eddy simulation study, Physics of Fluids, 36, 095 180, https://doi.org/10.1063/5.0226544, 2024.

Réthoré, P.-E., van der laan, M. P., Troldborg, N., Zahle, F., and Sørensen, N. N.: Verification and validation of an actuator disc model, Wind Energy, 17, 919–937, https://doi.org/10.1002/we.1607, 2014.

Sørensen, N. N.: General purpose flow solver applied to flow over hills, phd, Risø National Laboratory, 1995.

Sørensen, N. N.: EllipSys2D/3D User Manual, Tech. rep., DTU Wind Energy, Roskilde, Denmark, https://ellipsys.pages.windenergy.dtu.dk/docs/main.html, 2018.

Sørensen, N. N., Bechmann, A., Johansen, J., Myllerup, L., Botha, P., Vinther, S., and Nielsen, B. S.: Identification of severe wind conditions using a Reynolds Averaged Navier-Stokes solver, Journal of Physics: Conference Series, 75, 012 053, https://doi.org/10.1088/1742-6596/75/1/012053, 2007.

Troen, I. and Petersen, E. L.: European wind atlas, Risø National Laboratory, Roskilde, Denmark, 1989.

Troldborg, N., Sørensen, N., Réthoré, P.-E., and van der Laan, M. P.: A consistent method for finite volume discretization of body forces on collocated grids applied to flow through an actuator disk, Computers & Fluids, 119, 197–203, https://doi.org/10.1016/j.compfluid.2015.06.028, 2015.

Troldborg, N., Andersen, S. J., Hodgson, E. L., and Meyer Forsting, A.: Brief communication: How does complex terrain change the power curve of a wind turbine?, Wind Energy Science, 7, 1527–1532, https://doi.org/10.5194/wes-7-1527-2022, 2022.

van der Laan, M. P., Sørensen, N. N., Réthoré, P.-E., Mann, J., Kelly, M. C., and Troldborg, N.: The k-ϵ-fp model applied to double wind turbine wakes using different actuator disk force methods, Wind Energy, 18, 2223–2240, https://doi.org/10.1002/we.1816, 2014.

van der Laan, M. P., Sørensen, N. N., Réthoré, P.-E., Mann, J., Kelly, M. C., Troldborg, N., Hansen, K. S., and Murcia, J. P.: The k-ϵ-fP model applied to wind farms, Wind Energy, 18, 2065–2084, https://doi.org/10.1002/we.1804, 2015a.

van der Laan, M. P., Sørensen, N. N., Réthoré, P.-E., Mann, J., Kelly, M. C., Troldborg, N., Schepers, J. G., and Machefaux, E.: An improved k - ϵ model applied to a wind turbine wake in atmospheric turbulence, Wind Energy, 18, 889–907, https://doi.org/10.1002/we.1736, 2015b.

van der Laan, M. P., Andersen, S., Kelly, M., and Baungaard, M.: Fluid scaling laws of idealized wind farm simulations, Journal of Physics: Conference Series, 1618, 062 018, https://doi.org/10.1088/1742-6596/1618/6/062018, 2020.

Wagner, R., Courtney, M., Gottschall, J., and Lindelöw-Marsden, P.: Accounting for the speed shear in wind turbine power performance measurement, Wind Energy, 14, 993–1004, https://doi.org/10.1002/we.509, 2011.

Zengler, C. P., Troldborg, N., and Gaunaa, M.: Is the free wind speed sufficient to determine aerodynamic turbine performance in complex terrain?, Journal of Physics: Conference Series, 2767, 092 049, https://doi.org/10.1088/1742-6596/2767/9/092049, 2024.

Zengler, C. P., Troldborg, N., and Gaunaa, M.: Modeling the influence of streamwise flow field acceleration on the aerodynamic performance of an actuator disk, Wind Energy Science, 10, 1485–1497, https://doi.org/10.5194/wes-10-1485-2025, publisher: Copernicus GmbH, 2025a.

Zengler, C. P., Troldborg, N., and Gaunaa, M.: Predicting the impact of flow field acceleration on wind turbine performance in complex terrain and wind farms, Journal of Physics: Conference Series, 3016, 012 003, https://doi.org/10.1088/1742-6596/3016/1/012003, 2025b.